

Circulating mechanical power in a power-split hybrid electric vehicle transmission

M Schulz

Robert Bosch GmbH, Department FV/SLT, PO Box 30 02 40, 70442 Stuttgart, Germany.

email: Marcus.Schulz2@de.bosch.com

Abstract: Recently, a new power-split hybrid electric vehicle drivetrain has been developed by the Corporate Research and Development Department of the Robert Bosch company and two research cars equipped with this powertrain have been built. Owing to the loop-like arrangement of the shafts in the newly developed Dual-E Transmission, circulating power can arise in this system. In general, circulating power leads to high mesh losses because the power transmitted by some components becomes greater than the input or output power. This paper presents a detailed analysis of circulating power in the Dual-E Transmission. It is shown that the solution of the energy balance equations is given by a linear combination of four basic power flows. The factors in this linear combination, however, cannot be uniquely determined from the energy balance alone. Therefore, the transmission kinematics and dynamics are dealt with in detail. Subsequently, a mathematical description as well as a graphical representation of the circulating-power-free operating range are derived. This elaboration provides a solid basis for the development of a fuel-efficient operating strategy.

Keywords: hybrid electric vehicle, continuously variable transmission, circulating power, stop-start operation, regenerative braking, operating strategy, fuel consumption, fleet fuel economy, vehicle exhaust emissions

NOTATION

i	gear ratio
\bar{i}	overall transmission ratio
P_{E1}, P_{E2}	power inputs by electric motors E1 and E2 respectively
P_{ICE}	power input by the internal combustion engine
P_{OS}	power output
T	torques
λ_E	ratio of total mechanical power of electric machines to the transmission output power
ω	angular velocity

1 INTRODUCTION

Hybrid vehicles make use of two or more power plants. The concept of a hybrid electric vehicle (HEV) powered

by an internal combustion engine (ICE) and one or more electric motors has been well known for a long time [1]. During recent years, however, the interest of car manufacturers in HEVs has become stronger than ever. Many car makers developed research HEVs and displayed them at motor shows. Some even went a step further and introduced mass-produced HEVs to the market. In this respect, Toyota without doubt is a forerunner. After having launched the Toyota Prius as the first mass-produced hybrid electric passenger car in Japan in 1997 [2], 3 years later it was also introduced in the USA and in Europe. Recently, the second generation of the Prius was launched.

One motivation for this development is the concern that has been raised in the scientific community and the public at large about the climate change caused by the increased use of fossil fuels. The environmental concerns are mirrored in gradually tightening requirements of national regulations with regard to the exhaust emission behaviour of cars. In the USA, additional average fuel economy standards, which provide requirements for automobile manufacturer sales fleet fuel economy, have been adopted. It might be possible that, in future, regulations of this kind will also be implemented in Europe. In this

The MS was received on 14 April 2004 and was accepted after revision for publication on 25 June 2004.

context, hybrids appear to be a promising near-term option for a fuel-efficient vehicle. Consequently, HEVs that have been developed were initially predominantly geared to a low fuel consumption affecting the design of the power units as well as the control of their interaction. Often the vehicle was engineered from the ground up for maximum efficiency [3]. Only recently have car makers begun to shift the accent slightly more to the driving pleasure aspect of HEVs, installing hybrid powertrains in sports utility vehicles (SUVs) and thereby improving their power performance [4, 5]. This elucidates the broad area of application of hybrid systems, causing different car makers to start to develop a single ‘practical’ hybrid drivetrain that fits into a variety of their vehicles [5].

Regarding the powertrain topology, series, parallel and power-split hybrids can be distinguished between [1]. Characteristic for an HEV of the power-split type is that power from the ICE can be split into two parts, one of which is delivered to the wheels via a purely mechanical path and the other via an electrical path with one electric machine working as a generator and feeding another that works as a motor. The parallel arrangement of a mechanical transmission path consisting of common gear pairs or epicyclic gears and a non-mechanical path allows the construction of a continuously variable transmission. This principle is also known from hydrostatic mechanical transmissions [6]. The Prius is the most prominent representative of HEVs of this kind. Other examples are given in references [7] and [8]. Apart from fuel saving by stop–start operation of the ICE and regenerative braking, fuel-efficient operation of the power plants is facilitated by the possibility of continuously varying the transmission ratio.

Control of the mechanical, electrical and thermal (COMET) power train that has been developed by the Research and Development Department of the Robert Bosch company is shown in Fig. 1. It is a power-split hybrid electric drivetrain consisting of a gasoline or diesel ICE and the newly developed Dual-E Transmission. Together with a 42 V electrical system and a nickel–metal hydride (NiMH) traction battery pack, it has been fitted into a common mid-size saloon with rear wheel drive.

The Dual-E Transmission depicted in Fig. 2 consists of an input and output shaft, two countershafts, two identical epicyclic gears and asynchronous machines of

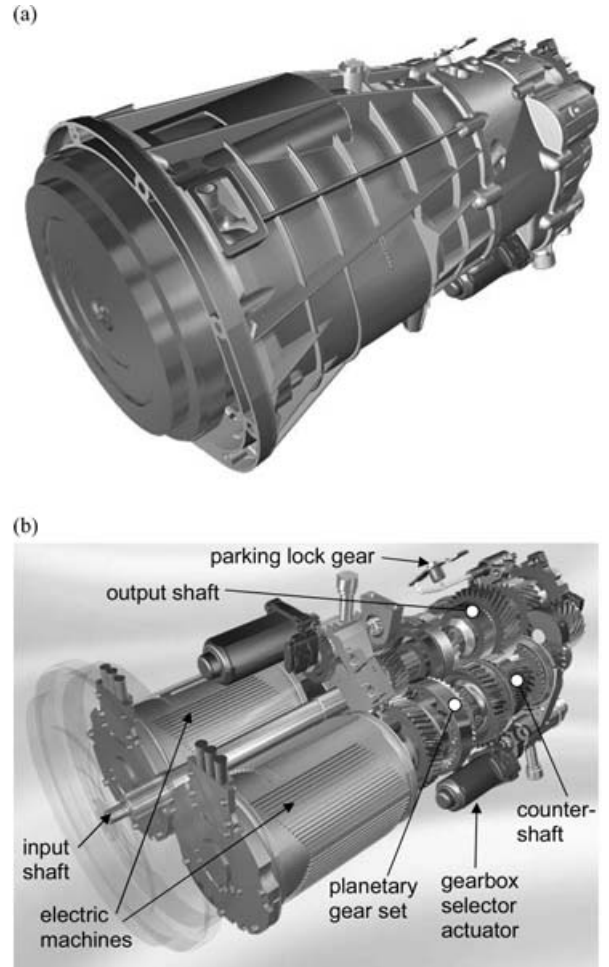


Fig. 2 Dual-E Transmission: (a) gearbox housing; (b) internal view

8 kW rated power each. The arrangement of the components becomes clear from the schematic diagram in Fig. 3. During the hybrid drive mode, typically, two gears of the countershafts are in mesh: one gear on countershaft L and one gear on countershaft H. The drive range is selected according to an overall operating strategy and the choice is made between the five drive ranges given in Table 1. Gear changes, if necessary, are performed automatically without traction interruption. In all the drive ranges, the overall transmission ratio is continuously variable.

It is known from complicated gear systems that the power transmitted by some components can become greater than the input or output power [9]. In those

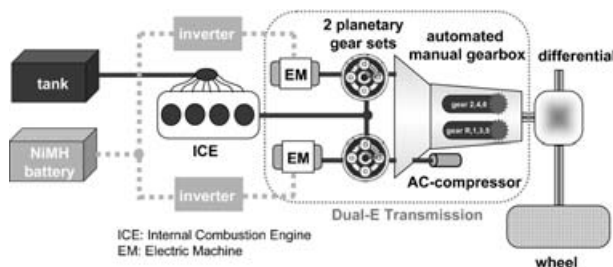


Fig. 1 COMET drivetrain

Table 1 Drive ranges

Drive range	Gear on shaft L	Gear on shaft H
1	1	2
2	3	2
3	3	4
4	5	4
5	5	6

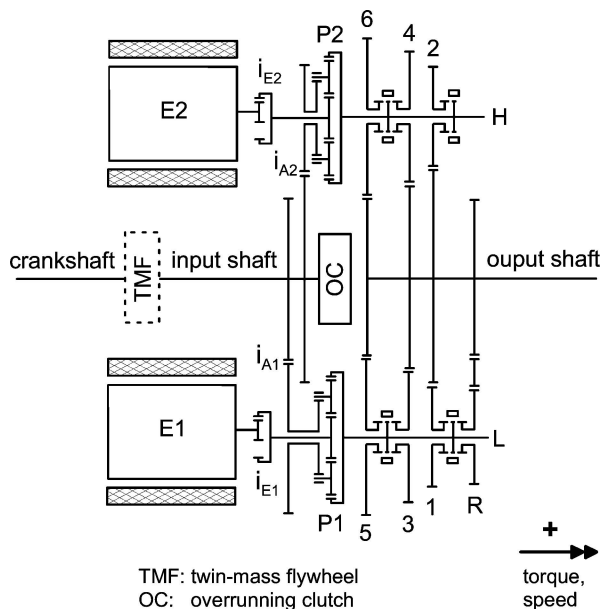


Fig. 3 Schematic representation of the Dual-E Transmission

cases, the circulating power incurred in the system can lead to high mesh losses and thereby to a low efficiency of the power transmission. The loop-like arrangement of the shafts in the Dual-E Transmission gives rise to the supposition that such effects may also occur in this system. Assuming that, in principle, circulating power can arise, it would be important to know the operating range that is free from it: this knowledge would be essential for developing a strategy leading to a fuel-efficient vehicle operation and avoiding the operation of the transmission in a range with high mesh losses. In particular, in the case of an HEV concept that is geared to a low fuel consumption, a high power loss of the transmission can render a design useless.

This paper presents a detailed analysis of circulating power in the Dual-E Transmission. In section 2, the energy balance equations are derived for the Dual-E Transmission and it is shown that their solution can be expressed by a linear combination of four basic power flows. Because it is not possible to determine all the factors of the linear combination from the energy balance alone, a detailed investigation of the kinematics and dynamics follows in section 3. On this basis, a mathematical description and a graphical representation of the circulating-power-free operating range are derived in section 4. A brief summary and outlook concludes the paper.

2 ENERGY BALANCE AND CIRCULATING POWER

Figure 4 depicts the internal and external power flow of the Dual-E Transmission. The ICE and the two electric machines E1 and E2 provide the mechanical power

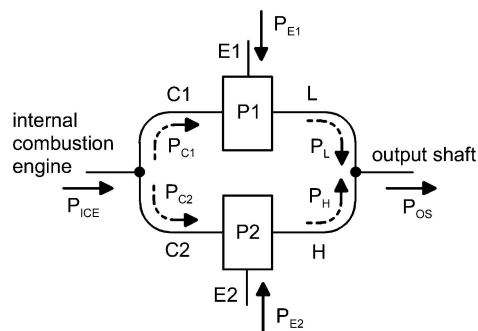


Fig. 4 Internal and external power flow of the Dual-E Transmission

input to the Dual-E Transmission P_{ICE} , P_{E1} and P_{E2} respectively. Together with the mechanical output power P_{OS} they represent the external power flow. The power of the combustion engine is split into power P_{C1} and P_{C2} driving the carriers C1 and C2 of the two epicyclic gears P1 and P2 respectively. The outputs P_L and P_H from ring gears R1 and R2 drive the two countershafts L and H. The internal power flow is represented by P_{C1} , P_{C2} , P_L and P_H . Neglecting inertia effects, compliance of the members and mechanical power loss, the energy balance can be formulated by the linear algebraic equations

$$Ax = b \tag{1}$$

with

$$A = \begin{bmatrix} 1 & 1 & 0 & 0 \\ 0 & 0 & 1 & 1 \\ -1 & 0 & 1 & 0 \\ 0 & -1 & 0 & 1 \end{bmatrix} \tag{2}$$

$$x = [P_{C1} \ P_{C2} \ P_L \ P_H]^T \tag{3}$$

$$b = [P_{ICE} \ P_{OS} \ P_{E1} \ P_{E2}]^T \tag{4}$$

The coefficient matrix A is singular. A thorough analysis shows that each solution can be expressed as a linear combination of three basic solutions depicted in Fig. 5 plus a cyclic power flow shown in Fig. 6. The three external power flows of Fig. 5 are a basis for the range of the coefficient matrix (2); the internal power flow of Fig. 6 spans the one-dimensional null space of this matrix.

It is noteworthy that the solutions in Fig. 5 exhibit a certain symmetry. In the case of the first two solutions, the external power flow is symmetric to the horizontal, and this symmetry is mirrored in the symmetry of the internal power flow. The external power flow of the third solution is symmetric to the vertical and so is the internal power flow. Owing to this symmetry, the mesh equation $P_L + P_{C1} - P_{C2} - P_H = 0$ holds for the three basic solutions and an arbitrary linear combination of them, but not so for the ‘circulating’ internal power flow P_O shown in Fig. 6.

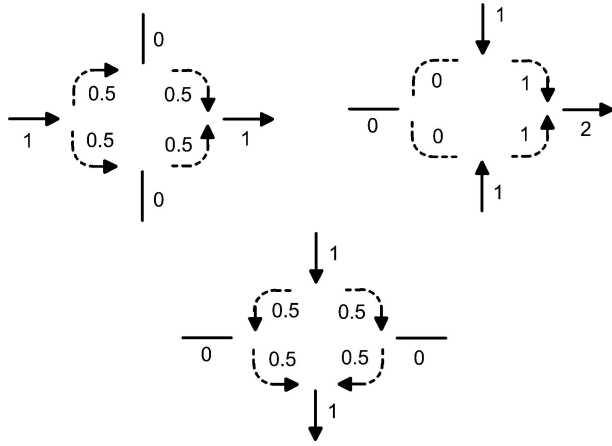


Fig. 5 Power flow: three symmetric basic solutions

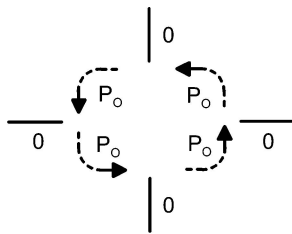


Fig. 6 Circulating power

In general, an internal power flow is called ‘circulating’ if the power flow through all the components C_1 , C_2 , L and H is directed in the same sense, either clockwise or counter-clockwise. This condition is different from $P_o \neq 0$, which can be seen by considering the following example. The fundamental solution 1 in Fig. 5 is neither circulating according to the definition given nor does $P_o \neq 0$. If the cyclic power flow in Fig. 6, however, is added to it with $-0.5 \leq P_o \leq 0.5$, it is still non-circulating with respect to the definition given, although it contains a component with $P_o \neq 0$.

For a given external power flow lying in the range of the coefficient matrix (2), the factors of the linear combination of the basic solutions shown in Fig. 5 can be determined uniquely. The factor P_o of the solution shown in Fig. 6, however, can be chosen arbitrarily. That means that the internal power flow is not uniquely defined by equations (1) to (4) alone, but a detailed investigation of the kinematics and dynamics of the transmission becomes necessary.

This is illustrated by Fig. 7 comparing two different internal power flows but with the same external power flow. Furthermore, assuming all the values P_1 to P_4 to be positive, the diagram on the left-hand side exhibits a circulating power flow enlarging the values of the internal power at all of the components C_1 , C_2 , L and H in the diagram on the left-hand side and, therefore, the circulating power flow would generate higher mesh losses. That is the reason why a circulating power flow should be avoided. From Fig. 7 it also becomes clear

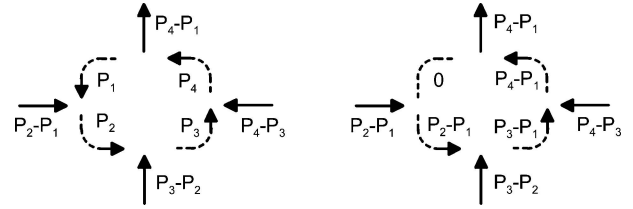


Fig. 7 Energy balance: indeterminate internal power flow

that, for a non-circulating power flow according to the definition given, it is impossible to reduce all the values of the internal power at the same time under the condition that energy balance (1) is satisfied and the external power flow remains unchanged. Some of the values can be reduced, but then the others are enlarged. Various other conditions, e.g. $P_o = 0$, which would also ensure this feature, can be thought of. However, all these conditions are stricter because they imply additional features. For example $P_o = 0$ implies the afore-mentioned mesh equation. Thus, the weakest condition has been chosen in the present paper.

3 KINEMATICS AND DYNAMICS

3.1 The epicyclic gear

For an epicyclic gear, the three angular speeds ω_s , ω_c and ω_r of the sun gear S , the carrier C and the ring gear R respectively are constrained by one linear relationship

$$\omega_c(1 - i_0) = \omega_s - i_0\omega_r \tag{5}$$

where $i_0 = -z_r/z_s$ is the ratio of the planetary gear set with the number z_r of teeth of the ring gear and the number z_s of teeth of the sun gear. The situation can be visualized by the nomograph shown in Fig. 8. For each of the angular velocities, one vertical axis is introduced. The ordinate of the carrier speed lies between the two other ordinates and divides the distance between the outer axes in the ratio of 1 to $-i_0$. The linear relationship (5) can be visualized as a straight line intersecting the three vertical axes. The values of the angular velocities

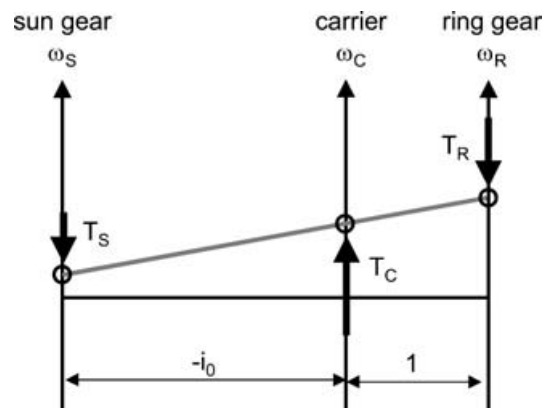


Fig. 8 Nomograph for the epicyclic gear

are defined by the corresponding intersection points. Therefore, varying the velocity state of the epicyclic gear corresponds to a translation and/or rotation of the straight line. Neglecting inertia effects and the power loss of the planetary gear set, the torques T_S , T_C and T_R acting on the shafts of the sun gear, the carrier and the ring gear respectively can be pictured as loads that act along the vertical axes and are applied to the straight line. In this picture, the straight line works as a lever and the balance equations can be derived by simply writing down the lever law.

3.2 Dual-E Transmission

Combining the kinematic equations (5) of the two epicyclic gears with the constraints imposed by the meshing gears, equations for the angular velocities ω_{E1} and ω_{E2} of the electric machines, depending on the angular velocity ω_{ICE} of the combustion engine and the angular speed ω_{OS} of the output shaft, can be derived. For example, with $i_{A1} = \omega_{ICE}/\omega_{C1}$, $i_{E1} = \omega_{E1}/\omega_{S1}$ and $i_L = \omega_{R1}/\omega_{OS}$, for the lower gear train

$$\frac{\omega_{ICE}}{i_{A1}}(1 - i_0) = \frac{\omega_{E1}}{i_{E1}} - i_0 i_L \omega_{OS}$$

or

$$\omega_{E1} = -c_1 \omega_{ICE} + c_2^{(L)} \omega_{OS} \tag{6}$$

Analogously, for the upper gear train

$$\omega_{E2} = -c_3 \omega_{ICE} + c_4^{(H)} \omega_{OS} \tag{7}$$

with the short cuts

$$\begin{aligned} c_1 &= -i_{E1} \frac{1 - i_0}{i_{A1}}, & c_2^{(L)} &= i_{E1} i_0 i_L \\ c_3 &= -i_{E2} \frac{1 - i_0}{i_{A2}}, & c_4^{(H)} &= i_{E2} i_0 i_H \end{aligned} \tag{8}$$

The values of all gear ratios are given in Table 2. Since the number of terminal shafts (ICE, E1, E2 and OS) is four, whereas the number of constraints (6) and (7) is two, the rotational degree of freedom is equal to $4 - 2 = 2$. Thus, the engine speed can be chosen independently of the current vehicle speed. Transmissions of such kind are referred to as infinitely variable or continuously variable transmission.

Neglecting mechanical losses and the inertia of the transmission components, the application of the principle of virtual power to the Dual-E Transmission gives

$$T_{ICE} \delta\omega_{ICE} + T_{E1} \delta\omega_{E1} + T_{E2} \delta\omega_{E2} + T_{OS} \delta\omega_{OS} = 0 \tag{9}$$

with the virtual angular speeds $\delta\omega_{ICE}$, $\delta\omega_{E1}$, $\delta\omega_{E2}$ and $\delta\omega_{OS}$ and the torques T_{ICE} , T_{E1} and T_{E2} that are applied by the combustion engine and the electric machines to the corresponding terminal shafts. The torque T_{OS} acting on the output shaft results from the road resistance (rolling and drag) and the inertia force of the vehicle. Note that the angular speeds and the torques are positive for the sense defined in Fig. 3.

The virtual angular speeds are subjected to the same constraints (6) and (7) as the real speeds. Substitution of the constraints into equation (9) yields

$$\begin{aligned} (T_{ICE} - c_1 T_{E1} - c_3 T_{E2}) \delta\omega_{ICE} \\ + (T_{OS} + c_2^{(L)} T_{E1} + c_4^{(H)} T_{E2}) \delta\omega_{OS} = 0 \end{aligned} \tag{10}$$

Since the virtual speeds $\delta\omega_{ICE}$ and $\delta\omega_{OS}$ in equation (10) are independent, the two expressions in parentheses must be zero and hence

$$T_{ICE} = c_1 T_{E1} + c_3 T_{E2} \tag{11}$$

$$-T_{OS} = c_2^{(L)} T_{E1} + c_4^{(H)} T_{E2} \tag{12}$$

4 ANALYSIS OF CIRCULATING POWER

According to the definition given in section 2, a mathematical condition for the occurrence of circulating power is $P_{C1} P_L > 0 \wedge P_{C2} P_H > 0 \wedge P_L P_H < 0$ (see Fig. 4). Note that this condition implies that $P_{C1} P_{C2} < 0$. By logical negation a condition for non-circulating power is

$$P_{C1} P_L \leq 0 \vee P_{C2} P_H \leq 0 \vee P_L P_H \geq 0 \tag{13}$$

In the following, it is assumed that on shaft L only one of the gears 1, 3 and 5 is selected but not the reverse gear (Fig. 3). Then, for positive engine speed and output speed the angular velocities of both ring gears R1 and R2 and of both carriers C1 and C2 are negative. Referring to Fig. 8, the lever law requires either that the torques on the planetary carrier C1 (C2) and on the ring gear R1 (R2) act in opposite directions or that they are zero together with the torque on the sun gear. Because power is obtained from the product of speed and torque,

Table 2 Gear ratios i

i_0	i_{A1}	i_{A2}	i_{E1}	i_{E2}	i_L			i_H		
					i_1	i_3	i_5	i_2	i_4	i_6
-42/12	-45/18	-40/23	44/11	30/11	-35/19	-24/27	-18/42	$= i_1$	$= i_3$	$= i_5$

the power P_{C1} (P_{C2}) of the carrier C1 (C2) and the power P_{R1} (P_{R2}) of the ring gear R1 (R2) have opposite signs or are both zero. With $P_{R1} = -P_L$ and $P_{R2} = -P_H$, it follows that

$$P_{C1}P_L \geq 0 \tag{14a}$$

and

$$P_{C2}P_H \geq 0 \tag{14b}$$

The equal signs imply torque-free planetary gears, and thus $P_L = 0$ or $P_H = 0$. Therefore, condition (13) can be reduced to $P_L P_H \geq 0$. Because the rotational speeds of shafts L and H have the same sign, $T_L T_H \geq 0$ or $T_{R1} T_{R2} \geq 0$. From the lever law requiring T_{R1} (T_{R2}) and T_{S1} (T_{S2}) to act in the same direction, finally, the following simple condition for a circulating-power-free operation can be deduced

$$T_{E1} T_{E2} \geq 0 \tag{15}$$

For a graphical representation of the operating range free from circulating power, it is useful to introduce the ratio of the total mechanical power of the electric machines to the output power

$$\lambda_E = \frac{P_{E1} + P_{E2}}{P_{OS}} \tag{16}$$

With $P_{E1} + P_{E2} = -P_{ICE} + P_{OS}$ (see Fig. 4) and $P_{ICE} = T_{ICE}\omega_{ICE}$, $P_{OS} = -T_{OS}\omega_{OS}$ and equation (11), it follows that

$$\lambda_E = 1 - c_1 \frac{T_{E1}}{-T_{OS}} \frac{\omega_{ICE}}{\omega_{OS}} - c_3 \frac{T_{E2}}{-T_{OS}} \frac{\omega_{ICE}}{\omega_{OS}} \tag{17}$$

For $\lambda_E > 0$ the vehicle typically is in one of the following two operating modes:

- (a) car propulsion ($P_{OS} > 0$) and power boost with the aid of the electric machines ($P_{E1} + P_{E2} > 0$);
- (b) regenerative braking ($P_{OS} < 0$ and $P_{E1} + P_{E2} < 0$).

For $\lambda_E < 0$:

- (c) car propulsion ($P_{OS} > 0$) and current generation ($P_{E1} + P_{E2} < 0$);
- (d) vehicle coasting to stop ($P_{OS} < 0$) with ignition turned off or engine start ($P_{E1} + P_{E2} > 0$).

The boundary of the circulating-power-free operating range is given by the limiting case $T_{E1} T_{E2} = 0$ of the inequality condition (15), i.e. either $T_{E1} = 0$ or $T_{E2} = 0$. For $T_{E1} = 0$, equation (17) together with equation (12) give

$$\lambda_E = 1 - \frac{c_3}{c_4^{(H)}} \frac{\omega_{ICE}}{\omega_{OS}} \tag{18}$$

and, for $T_{E2} = 0$,

$$\lambda_E = 1 - \frac{c_1}{c_2^{(L)}} \frac{\omega_{ICE}}{\omega_{OS}} \tag{19}$$

The linear relationships (18) and (19) between λ_E and the overall transmission ratio $\bar{i} = \omega_{ICE}/\omega_{OS}$ are represented by two straight lines in Fig. 9.

So far, it is open whether the area between the two half-lines represents the operating range free from or associated with circulating power. The answer can be found, for example, by evaluating criterion (15) at a single point of the (\bar{i}, λ_E) plane, e.g. the point halfway between the crossing points of the half-lines with the axis $\lambda_E = 0$: $\bar{i} = \frac{1}{2}(c_2^{(L)}/c_1 + c_4^{(H)}/c_3)$. Evaluation of the kinematic equations (6) and (7) at this point leads to

$$\frac{\omega_{E1}\omega_{E2}}{\omega_{OS}^2} = -\frac{1}{4}c_1c_3\left(\frac{c_2^{(L)}}{c_1} - \frac{c_4^{(H)}}{c_3}\right)^2 \tag{20}$$

and, as $c_1 > 0$ and $c_3 > 0$, it follows that $\omega_{E1}\omega_{E2} < 0$. Together with $\lambda_E = 0$, finally, $T_{E1}T_{E2} > 0$. Thus, the area between the two half-lines in Fig. 9 represents the operating range free from circulating power. For each of the drive ranges given in Table 1, similar graphical representation of the operating conditions free from circulating power is obtained. As shown in Fig. 10, the areas for neighbouring drive ranges are adjacent and have one boundary in common. This is because either on shaft L or on shaft H the same gear is put into mesh for neighbouring drive ranges (see Table 1).

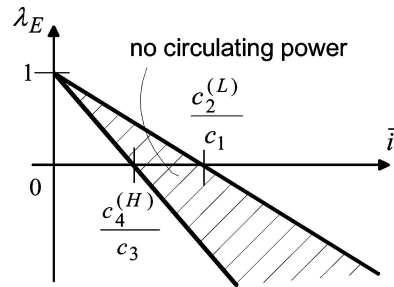


Fig. 9 Operating range free from circulating power

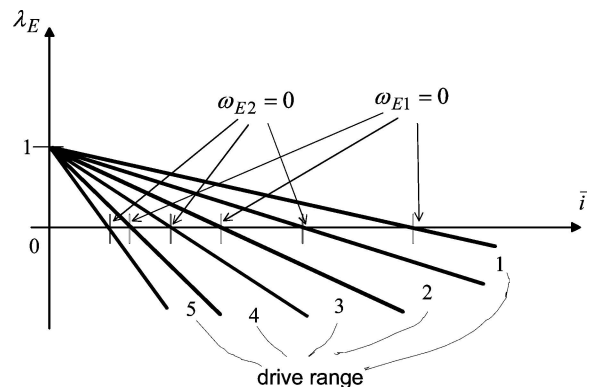


Fig. 10 Synopsis of circulating-power-free operating ranges

5 CONCLUSIONS

Energy balance equations have been derived for the newly developed HEV Dual-E Transmission. It has been shown that their solution can be expressed as a linear combination of four basic power flows. Since the factors of the basic solutions cannot be uniquely determined from the energy balance alone, the transmission kinematics and dynamics have been dealt with in detail. One of the basic solutions is associated with a circulating power flow. For each of the five drive ranges the circulating-power-free operating range is represented by an angle between two half-lines in the (\bar{i}, λ_E) plane, with the overall transmission ratio \bar{i} and the ratio λ_E of the total mechanical power of the electric machines to the output power. For neighbouring drive ranges, the corresponding angles are adjacent and have one side in common. On the basis of this knowledge, a fuel-efficient operating strategy can be developed for the COMET car, taking into account that circulating power leads to high mesh losses. Indeed, such a strategy has been implemented on two HEV prototypes that have been built by the Corporate Research and Development Department of the Robert Bosch company. In a first version of the control strategy, vehicle operation is permitted only in the circulating-power-free range. A more sophisticated version incorporates a detailed model of the mechanical transmission losses based on experimental data. By simulation, as well as by experiments that will be presented in a forthcoming paper, it can be verified, however, that the difference between the operating points obtained by the two strategies is relatively small. For the Dual-E Transmission, therefore, the simpler strategy avoiding the occurrence of circulating power turns out to be a suitable approach.

ACKNOWLEDGEMENT

The present author particularly thanks one of the anonymous referees for his detailed comments and suggestions. The exposition has been much improved by these suggestions.

REFERENCES

- 1 Wallentowitz, H., Biermann, J.-W., Bady, R. and Renner, C. Strukturvarianten von Hybridantrieben. *VDI-Tagung 'Hybridantriebe'*, Munich, Germany, 1999.
- 2 Abe, S. Toyota Motor Corporation (contributor) Toyota Prius: best engineered car of 2001. *Automot. Engng Int.*, March 2001, 27–35.
- 3 Baun, R. Der Honda Insight. *Automobiltechnische Z.*, 2000, **102**, 226–227.
- 4 Jost, K. Dodge power box hybrid SUV. *Automot. Engng Int.*, March 2001, 12–14.
- 5 Jost, K. A new ParadiGM in hybrid powertrains. *Automot. Engng Int.*, March 2001, 37–38.
- 6 Jarchow, F. Stufenlos wirkende hydrostatisch–mechanische Lastschaltgetriebe. *VDI Ber.*, 1991, **878**, 623–647.
- 7 Tenberge, P. Electric–mechanical hybrid transmission. In Proceedings of the International Congress on *Continuously Variable Power Transmission*, Eindhoven, The Netherlands, 1999, pp. 196–201.
- 8 Tenberge, P. E-Automat—Automatikgetriebe mit Esprit. *VDI Ber.*, 2001, **1610**, 455–480.
- 9 Dooner, D., Yoon, H.-D. and Seireg, A. Kinematic considerations for reducing the circulating power effects in gear-type continuously variable transmissions. *Proc. Instn Mech. Engrs, Part D: J. Automobile Engineering*, 1998, **212**(D6), 463–478.